FRACTURE PROCESS ZONE IN CONCRETE: A THREE DIMENSIONAL GROWTH PROCESS

J.G.M. van Mier*

Results of vacuum impregnation tests on concrete single-edge-notched specimens subjected to uniform boundary displacement are presented. The tensile fracturing of the specimens is a highly non-uniform three dimensional process involving discontinuous crack growth and crack interface grain bridging. An 'intact core' was detected in some of the specimens. The influence of maximum aggregate size on the load-deformation response in tension could be explained from crack interface grain bridging. The increased carrying capacity in cracks in coarse grained materials can be explained from the increased size of the crack interface grain bridges. The grain bridges reflect an internal length scale of the material, and the experiments validate the introduction of higher order strain terms and the associate internal length in continuum models for localization.

INTRODUCTION

The heterogeneity of concrete and other composites results in highly non-linear fracture behaviour. Based on an analogy with the Dugdale/Barenblatt model for fracture of plastic metals, the fictitious crack model (1) and the crack band model (2) were developed for concrete. The plastic crack tip zone was simply regarded as an extensive zone of diffuse microcracking. However, the existence of such a zone of microcracks in front of a macrocrack tip (3) has never been confirmed experimentally. Because the mechanical behaviour of concrete is strongly affected by temperature and moisture effects (non-uniform drying leads to eigenstresses in the specimens), surface crack measurements are not representative for the internal cracking of the specimen. In this paper results of a number of vacuum impregnation tests on single edge notched concrete plates subjected to uniform boundary displacement are presented. Rather than trying to identify a macrocrack tip and a cloud of microcracks, the global 'crack status' of a specimen was matched with subsequent stages in load-deformation response. The results clearly revealed the three dimensionality of the fracture process in concrete involving discontinuous crack growth and crack interface grain bridging.

* Delft University of Technology, Department of Civil Engineering, Stevin Laboratory, P.O.Box 5048, 2600 GA Delft, The Netherlands.

IMPREGNATION EXPERIMENTS

Dye penetration tests on concrete three point bend specimens have been carried out before, e.g. (4). These tests revealed that the beams fracture along a curved-crack front with a longer crack length at the surfaces as compared to the crack extension in the centre of the specimen. In the current approach single-edge-notched specimens (SEN) were used and subjected to uniform boundary displacement. The typical response of the SEN geometry allows for an inproved understanding of the details of the fracture process.

Specimens and Technique

SEN specimens of size 100 x 200 x 50 mm (see Fig. 1), were loaded in tension under uniform boundary displacement. The notch is a 5 mm wide, 15 mm deep sawcut. After loading a specimen in displacement control (the control parameter is the average axial deformation measured with the four corner LVDTs, see Fig. 1) up to a prescribed average axial deformation, the specimen was unloaded and fixed with steel bars between the glue platens in the tensile apparatus. Next, the specimen (with the glue platens still attached) was removed from the machine and placed in a small basin filled with a low viscosity (110 mpas at 23^0C) fluorescenting epoxy (CIBA-GEIGY EP-IS, 0.5 g BASF fluorol was added to 245 ml epoxy resin, pot-life appr. 1 hour). The basin was placed in a vacuum chamber, and vacuum (10 mbar) was maintained during 45 mins.

After impregnation, specimens were sawn in six parallel slices of 15 mm thickness. Internal cracking could now be detected under Ultra-Violet light. With this technique the extent of continuous macrocracks over the specimens cross-section can be studied, whereas the geometry of the crack in the loading direction is revealed as well. For obvious reasons, discontinuous microcracks cannot be visualised with the impregnation technique. Cracking was recorded using UV photography. The details of the photographic technique are explained in (5).

Variables

Variables in the investigation were the maximum aggregate size of the concrete (d_{max} = 2 or 16 mm), the LVDT control length (35 and 65 mm) and the maximum crack opening to which a specimen was loaded (10, 25, 50, 100 and 200 μm). In this paper only part of the results are shown: the effect of maximum aggregate size and the relation between crack opening and internal cracking of the specimens are presented.

Results

In Fig.2, the load-average crack opening (P-w) diagrams of two 2 mm experiments and two 16 mm experiments are shown. For each mix, the results of the specimens loaded up to 25 and 100 μm respectively are included in this graph. The peak-load, the actual unloading deformation and the residual load measured in the four experiments are gathered in Table 1. The extent of cracking in specimens pertaining to the two mixes at an average crack opening of 25 and 50 μm respectively are shown in Figs. 3 and 4.

TABLE 1 - Peak loads, Unloading Deformations and Residual Loads Measured in the Four Impregnation Tests of Fig. 2.

Specimen number	Code	Control length	d_a [mm]	P_{max} [kN]	w_{unl} [μm]	P_{unl} [kN]
1	16A012	35	2	11.14	24.6	2.91
2	14A007	35	2	11.99	109.4	0.60
3	41A025	35	16	9.87	23.9	5.93
4	45A034	35	16	9.98	97.0	1.81

DISCUSSION OF RESULTS

In the SEN specimens crack nucleation occurs at the notch, and under subsequent crack growth, the specimen will be loaded more and more excentric. Because the end faces are kept parallel to each other, the growing crack will be arrested in the generated bending moment. The growth of the crack is accompanied by a plateau in the load-deformation diagram. At a certain stage, the deformations at the 'unnotched' side of the specimen will exceed the maximum deformation capacity of the material, and the crack will 'jump' to the unnotched side (6). The length of the plateau depends on the actual specimen dimensions, whereas the slope of the P-w curve at the end of the plateau is governed by the elastic energy stored in the specimen and the heterogeneity of the material of which the specimen is made. The results of Fig. 3 reveal that cracking starts at the edges of the specimen, most likely due to non-uniform drying which cannot be avoided and confirms previous results (4). After the crack has jumped to the other side of the specimen, an intact core remains at average crack openings of 50 μm (Fig. 4). This core is not necessarily uncracked and distributed microcracks may be present while these cannot be visualized using the impregnation technique. The existence of distributed microcracks can however be deduced from crack photographs of the 16 mm specimen loaded up to 25 μm (Fig.5). The photographs show debonding near large aggregates close to the notch. The photographs reveal the complex crack geometry over the depth of a specimen (50 mm) at a distance x from the notched side of the specimen (x is defined in Fig. 1).

Although surface deformation measurements indicated that cracking started at the notch, the impregnation tests for the fine grained mix showed that continuous cracks appeared first at the other side of the specimen (see Fig. 3a and 6). Most likely the debonding cracks were too small to be detected in the 2mm experiments. The jump of the 'crack' (which is in fact a crack-like structure of debonding meso-cracks) to the unnotched side of the specimen is accompanied by a steep stress drop in the P-w diagram (6). The effect is most pronounced for the fine grained mix (test no.1 and 2 in Fig. 2), and is partly a specimen and partly a material effect. Due to the smaller size of the aggregates in the fine grained mix, the microcracks will be more subsceptible to coalescence. Recently it was shown that crack coalescence leads to snap-back behaviour (e.g. (7)), which may enhance the steep slope of the softening curve at average crack openings of 20 μm

for the fine grained material. In the coarse grained mix these effects are smaller because the individual debonding cracks will not develop in the same plane (Fig. 5). The stress-redistributions are then less severe after the crack jump.

At 100 μm the cracks have completely traversed the specimens, yet Fig. 2 and Table 1 indicate that still a considerable load transfer is possible in the specimens. The effect can be explained from the development of intact crack interface grain bridges (when no crack coalescence occurs), which were observed both in the 2 and 16 mm specimens as shown in Fig. 7a-c. The increased load-carrying capacity in the tail of the softening curve ($w > 20\ \mu m$) can be explained from the increased size of the material bridges. Schematizing a grain bridge as a beam element (with span d_{max}, height d_{max} and unit thickness) with fixed supports, of which one has undergone a displacement w, it is found that the maximum stress in the 'beam' is equal to $3Ew/d_{max}$. When the aggregate size is increased by a factor 4 (as in the current experiments), the flexural stress decreases by a factor 4. In the experiments, the residual load was found to increase by a factor 3 when the aggregate size was increased by 4. The difference can probably be explained from the fact that no flexural failure of the grain bridges occurs. Instead the mechanism depicted in Fig. 7d seems to prevail. Recently it was found that numerical analyses of localization are more stable when higher order terms are included in the description of the strain field (8). The current experiments confirm that indeed an internal length exists during localization, and first estimates are that it is equal to the maximum aggregate size.

REFERENCES

(1) Hillerborg, A., Petersson, P.E. and Modeer, M., Cem. and Conc.Res., Vol.6, No.6, 1976, pp.773-782.

(2) Bazant, Z.P. and Oh, B.-H., Mat. and Struct., RILEM, Vol.16, No.93, 1983, pp.155-178.

(3) Mindess, S., in "Fracture Mechanics of Concrete - Test Method". Edited by S.P. Shah, Chapman & Hall, London/New York, 1990 (in print).

(4) Bascoul, A., Kharchi, F. and Maso, J.C., in "Fracture of Concrete and Rock". Edited by S.P. Shah and S.E. Swartz, Springer Verlag, New York, USA, 1989, pp.396-408.

(5) Van Mier, J.G.M., submitted to Cem. and Conc.Res., 1990.

(6) Van Mier, J.G.M. and Nooru-Mohamed, M.B., Eng.Fract.Mech., Vol.35, No.4/5, 1990, pp.617-628.

(7) Ortiz, M., Int.J. Solids Structures, Vol.24, No.3, 1988, pp.231-250.

(8) De Borst, R., in "Computer Aided Analysis and Design of Concrete Structures". Edited by N. Bicanic and H. Mang, Pineridge Press, Swansea, 1990, pp.931-943.

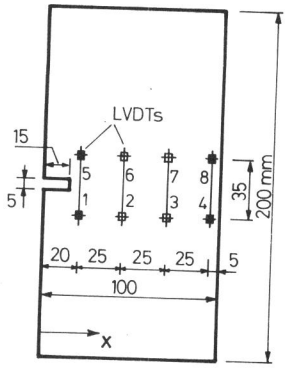

The control displacement is the average displacement measured with LVDT nos. 1, 4, 5 and 8.

Fig. 1. Specimen geometry with location of LVDTs.

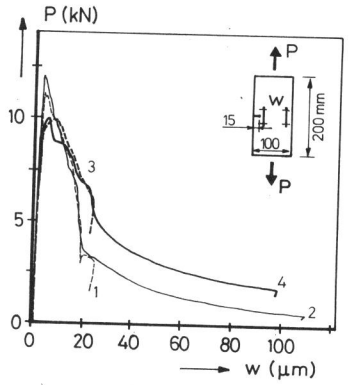

no. 1, 2: d_{max} = 2 mm
no. 3, 4: d_{max} = 16 mm

Fig. 2. Load-crack opening diagrams for the 2 and 16 mm mixes.

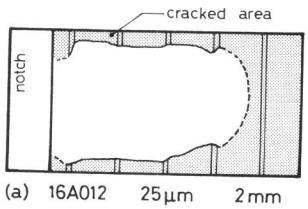

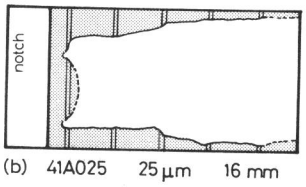

Fig. 3. Cracking in two 25 μm experiments no. 1 and 3.

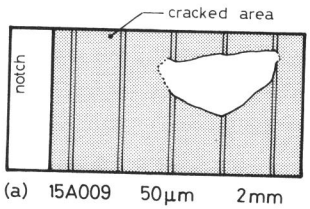

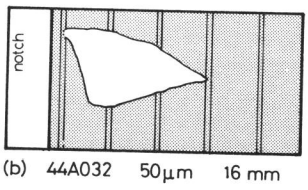

Fig. 4. Cracking in two 50 μm experiments.

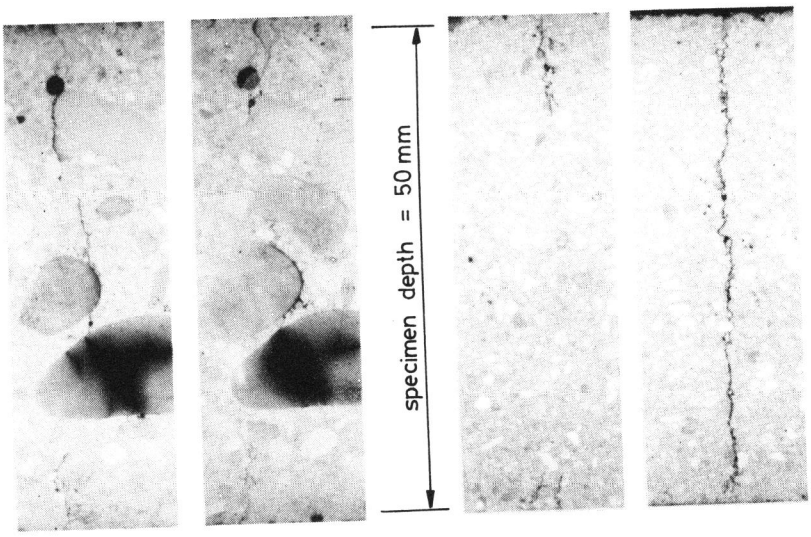

Fig. 5. Debonding near aggregates, 41A025 (3), $d_{max} = 16$ mm.

Fig. 6. Continuous cracks in specimen 16A012 (1), w = 25 μm.

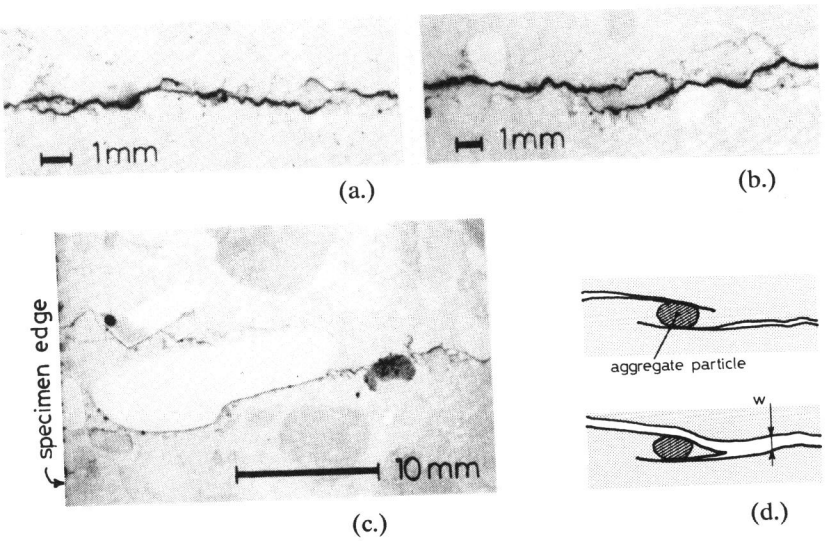

Fig. 7. Crack interface grain bridging at w = 100 μm in 2 mm mortar (a., b.) and 16 mm concrete (c.); and bridge failure mechanism (d.).